Catalysis Communications 187 (2024) 106844

Contents lists available at ScienceDirect

Catalysis Communications

journal homepage: www.elsevier.com/locate/catcom

Efficient activation of peroxymonosulfate with zirconia-supported manganese and cobalt catalysts for oxidation of ibuprofen

Romina D. Goenaga, Alejandra S. Diez, Mariana Alvarez *

INQUISUR, Departamento de Química - Universidad Nacional del Sur (UNS) - CONICET, Avda. Alem 1253, B8000CPB Bahía Blanca, Argentina

ARTICLE INFO

Keywords:
Zirconium oxide
Cobalt and manganese catalysts
Ibuprofen degradation
Peroxymonosulfate
Sulfate radical

ABSTRACT

This study assessed the efficacy of ZrO_2-based catalysts with different Mn(II) and Co(II) metal loadings for catalytic degradation of ibuprofen using peroxymonosulfate anion as oxidant. The support was prepared via co-precipitation, and metal ion deposition was achieved through incipient wetness impregnation. Catalysts were characterized by atomic absorption spectrometry, X-ray diffraction, Fourier-Transform infrared spectroscopy, and scanning electronic microscopy. Optimal experimental conditions resulted in complete ibuprofen degradation in 30 min, with 63.3% mineralization. The best-performing catalyst was reusable up to three times. Both sulfate and hydroxyl radicals were generated in the oxidant activation process.

1. Introduction

Pharmaceutical products are used to control some symptoms that are produced by different diseases [1]. Among these drugs, anti-inflammatories are the most widely used, leading to an increase in their production. Nonsteroidal anti-inflammatories (NSAIDs) are a group of pharmaceuticals that do not require a medical prescription and are globally used to treat various pathologies. Among them, ibuprofen (IBU, 2-(4-isobutylphenyl) propanoic acid) is a NSAIDs frequently prescribed as an antipyretic, analgesic and anti-inflammatory drug [2,3]. The high consumption of this compound has raised concerns about its potential environmental risks, because IBU has been detected in surface water and sewage effluents at ng/L and μg/L levels [4–6]. The main source of contamination of IBU could be attributed to the release through urine of the metabolized and non-metabolized drug by humans and animals, as well as waste from the chemistry and pharmaceutical industry and non-consumed expired drugs [7]. This poses a potential danger to human health and is ecotoxic to aquatic ecosystems, as IBU has harmful effects on various species including fungi, bacteria, algae, crustacean microorganisms and fish [4,7].

For all of the above reasons, IBU can be classified as an emerging pollutant (EP). It is well known that the EP can be found in bodies of water and could be potentially toxic as they tend to accumulate in aquatic organisms due to their low aqueous solubility and degradation resistance [8–10]. To date, there are different removal methods for IBU: physical methods as adsorption [11], chemical methods as ozonation [12] photodegradation [1] and biodegradation [13]. However, these methods are often inefficient for the elimination of IBU or do not achieve its complete degradation. The complete mineralization of this compound is a keypoint objective to be reached, since the by-products generated after its oxidation could be more toxic than the IBU parent molecule. For this reason, Advanced Oxidation Processes (AOPs) appear as an attractive alternative for IBU degradation. AOPs are a family of techniques that present numerous advantages for the degradation of pharmacological compounds in aqueous solutions such as, high efficiency, non-selectivity and simple operation and low secondary contamination [14].

The AOPs are based predominantly on the generation of strongly oxidizing radicals (mainly $^{\bullet}OH$) that are used to degrade recalcitrant compounds, if possible until its complete mineralization. Within the typical AOP, the Fenton reaction has been widely studied for the elimination of these type of compounds, but this technique has some disadvantages such as the formation of acid sludge and the use of H_2O_2, which can be harmful to workers [15]. Therefore, an innovative alternative is to use Advanced Oxidation Processes based on sulfate radicals (Sulfate Radical-based Advanced Oxidation Processes, SR-AOP).

Compared to AOPs based on $^{\bullet}OH$ radicals, SR-AOPs offer numerous advantages. For example, standard reduction potential of $SO_4^{\bullet-}$ (E^0 = 2.5–3.1 V) is similar to that of $^{\bullet}OH$ (E^0 = 1.9–2.7 V), but the lifetime of $SO_4^{\bullet-}$ in water is longer. As a result, the degradation with sulfate radicals could lead to a better mineralization [16,17]. In addition, $SO_4^{\bullet-}$ radicals have a wider operating pH range than $^{\bullet}OH$, are more stable and more

* Corresponding author.
E-mail addresses: romina.goenaga@uns.edu.ar (R.D. Goenaga), alejandra.diez@uns.edu.ar (A.S. Diez), alvarezm@criba.edu.ar (M. Alvarez).

https://doi.org/10.1016/j.catcom.2024.106844
Received 26 September 2023; Received in revised form 4 December 2023; Accepted 9 January 2024
Available online 10 January 2024
1566-7367/© 2024 The Authors. Published by Elsevier B.V. This is an open access article under the CC BY-NC-ND license (http://creativecommons.org/licenses/by-nc-nd/4.0/).

Table 1
Parameters varied for process optimization.

Catalyst dose (g/ L)	0.667	1.33
Oxone® dose (g/ L)[a]	1.33	2.00
PMS dose (g/ L)	0.659	0.991

[a] Source of PMS.

Table 2
Chemical analysis and mean crystallite size of the catalysts.

Catalysts	Metal content (g%)		Crystallite size (nm)
	Co	Mn	
Co_2	2.14	–	34.2
Mn_2	–	1.19	35.5
Co_2Mn_2	1.33	1.35	22.4
Co_4	5.30	–	25.9
Mn_4	–	2.49	36.6

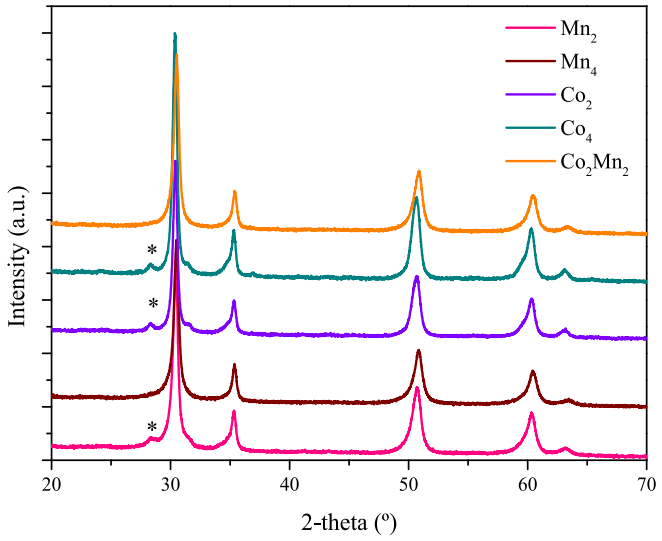


Fig. 1. XRD patterns of the prepared catalysts.

selective because they react mainly with organic compounds through an electron transfer mechanism [18]. These radicals can be produced in situ through the activation of persulfate (PS, $S_2O_8^{2-}$) or peroxymonosulfate (PMS, HSO_5^-) anions. PS is marketed as $Na_2S_2O_8$ or $K_2S_2O_8$, and PMS as a triple salt ($2KHSO_5{\cdot}KHSO_4{\cdot}K_2SO_4$) called Oxone® or Caroat® [19–22]. Another benefit of using these oxidants is that they exist in solid state at room temperature, are very stable, easy to transport and store and highly soluble in water (solubility of Oxone® in water (293 K): 29.8 g cm^{-3} [23], solubility of $K_2S_2O_8$ in water (293 K): 5.2 g cm^{-3} [24]).

Among the different methods available for the activation of oxidizing agents, the employment of heterogeneous metal catalysts offers numerous advantages: increases the production of radicals, making the process more effective in general and sustainable because it can be used for more than one reaction cycle, thus avoiding the difficulties associated with metal catalysts in homogeneous phase, among others [25,26].

Zirconium oxides (ZrO_2, henceforth Z) are very interesting materials to be applied as supports because of their chemical properties. In recent years, mono- and bimetallic modified Z have been reported for the degradation of IBU [27–29]. However, these articles describe the use of these catalysts for the degradation of dilute IBU solutions (10 ppm), using H_2O_2 as oxidant, with reaction temperatures ranging from 60 to 80 °C. Thus, to the best of our knowledge, there are few reports on the use of metals supported on Z for SR-AOP. For these reasons, we decided to investigate the activity of different Co and/or Mn catalysts supported on Z in the degradation of IBU in aqueous phase under mild reaction conditions.

2. Experimental

2.1. Synthesis of the support and catalysts

A series of mono and bimetallic Co and Mn catalysts were prepared employing Z as support. All chemicals used in this study were analytical grade reagents and were used as received without further purification. Distilled water was used in the present work.

The synthesis of the support was carried out following the technique described by Garcia et al. [30]. The precursor, zirconium hydroxide $Zr(OH)_4$, was precipitated from a solution of 0.4 M $ZrOCl_2{\bullet}8H_2O$ by dropwise addition of NH_4OH solution (28% NH_3) until pH 10, under vigorous stirring at room temperature. The precipitate was vacuum filtered and washed with distilled water. The obtained solid was dried in an oven at 373 K for 24 h.

The deposition of Co and/or Mn promoters (depending on the mono or bimetallic catalyst obtention) was carried out by the incipient wetness impregnation method. To this end, $Co(NO_3)_2$ and $Mn(NO_3)_2$ aqueous solutions were added dropwise to $Zr(OH)_4$, maintaining a solution:solid ratio of 0.4 mL/g. The concentration solutions were adjusted to obtain metal contents of 2.0% and 4.0% (m/v). The catalysts were then dried at 383 K for 24 h. Finally, all catalysts were calcined at 873 K for 4 h in air. Mono (Me_x) and bimetallic ($Me1_xMe2_y$) catalysts were prepared, where Me indicates the metal used in the impregnation and the subscripts x and y indicate the nominal percentage metal concentration.

2.2. Catalysts' characterization

The metal content in the samples was determined by atomic absorption spectrometry using a GBC Avanta Model B-932 atomic absorption spectrometer. Ten mg of solid were dissolved by means of the adding of adequate quantities of 12 M HCl and 50% HF.

X-ray diffraction experiments were performed in a Panalytical Empyrean diffractometer with CuKα1 radiation (λ = 0,15,406 nm), between 2θ = 15–80°.

Fourier-Transform infrared (FTIR) spectra of the samples were recorded in a FTIR-NIR Thermo Scientific Nicolet iS50, in the 400–4000 cm^{-1} region. Samples were pulverized and pellets were prepared in a hydraulic press using KBr in a 1:100 ratio.

The morphology of the prepared materials was evaluated by Scanning Electronic Microscopy (SEM) using a Carl Zeiss EVO MA 10 equipped with an energy dispersion spectrometer (EDS) Cambridge x-act. For the EDS analysis, a beam energy of 20 keV was employed.

X-ray photoelectron spectroscopy (XPS) spectra were collected in a PHI 548 spectrometer with a double pass cylindrical mirror analyzer, using non-monochromatic Al Kα radiation (1486.6 eV). High-resolution spectra of C 1 s, O 1 s, Co 2p, and Zr 3d were recorded, and the binding energies were recalibrated based on the C 1 s line at 284.8 eV. Spectra analysis and peak deconvolution were performed with OriginPro 9.0 software, using a polynomial spline baseline and a Gaussian function.

2.3. IBU degradation experiments

The degradation reactions were carried out at 303 K in a 100 mL jacketed glass reactor connected to a thermostatic bath. In the various experiments carried out, 75 mL of IBU solution (40 ppm) was brought into contact with the desired amount of catalyst and PMS oxidant. The oxidation process was optimized by evaluating the effects of different parameters (PMS dose, catalyst type and dose) as shown in Table 1.

In each case, the reaction was continued for at least 3 h or until complete consumption of the oxidant was detected, whichever occurred first. At predetermined intervals, 3 mL aliquots were withdrawn from the vessel with a syringe, and filtered through a cellulose acetate filter

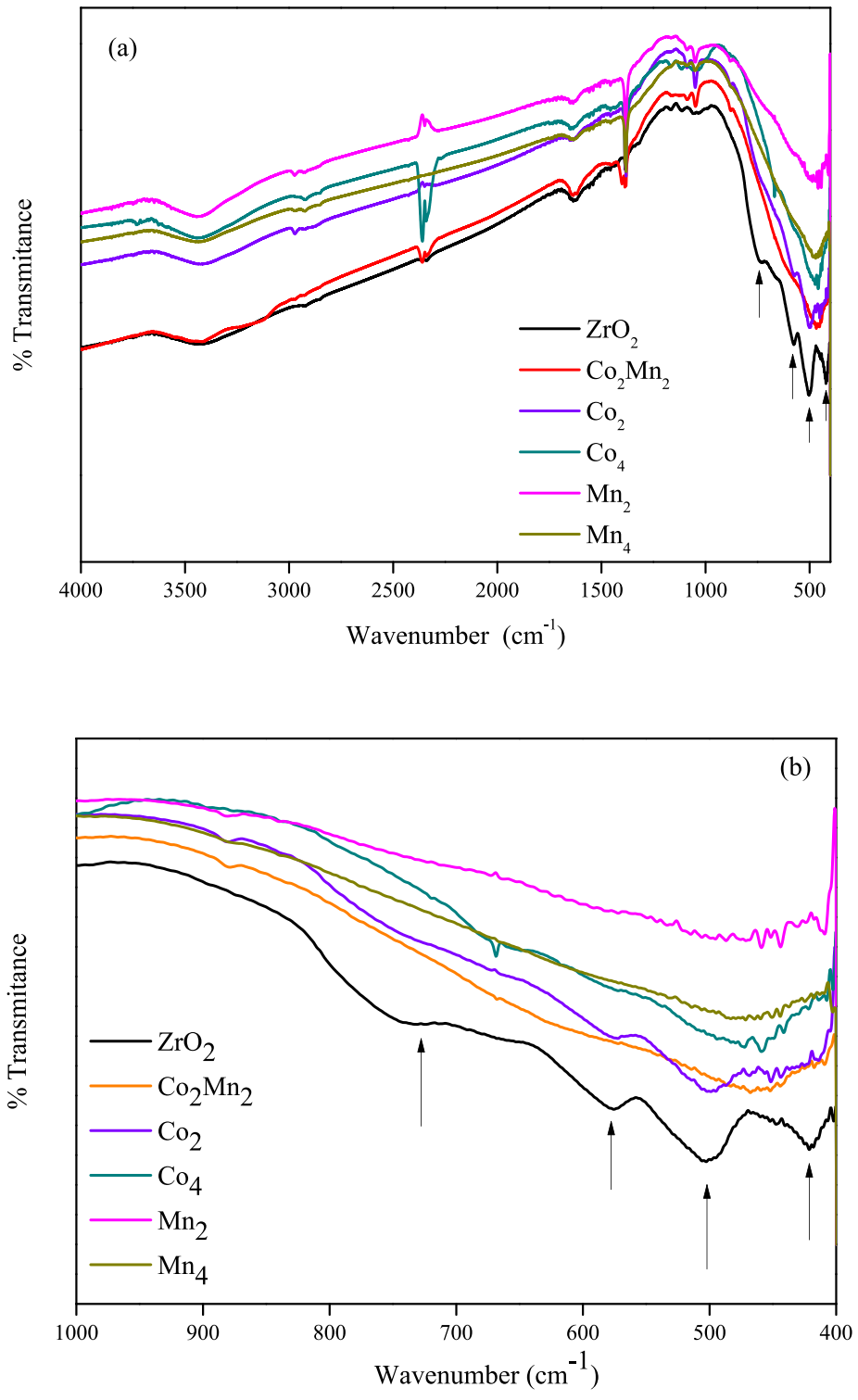


Fig. 2. (a) FTIR spectra at 4000–400 cm^{-1} and (b) expanded FTIR spectra at 1000–400 cm^{-1} of Z support and Co_2Mn_2, Mn_4, Co_4, Mn_2 and Co_2 catalysts.

(0.22 μm). The absorption spectrum of an IBU solution is characterized by an intense band with a maximum absorption wavelength (λ_{max}) at 221 nm, corresponding to the π-π* transition of the aromatic ring. The UV–Vis spectra (λ = 200–600 nm) of each aliquot were recorded using an Agilent Cary 50 UV–Vis spectrometer, in order to monitor the decrease in IBU concentration. Fluorescence spectroscopy using a Shimadzu RF-6000 spectrofluorometer was also used to evaluate the disappearance of IBU during the reaction. The fluorescence intensity was measured at λ_{em} = 282 nm, with an excitation wavelength of λ_{exc} = 219.8 nm.

The remaining PMS in the residual reaction liquid was determined by a colorimetric way, following the method proposed by Wacławek et al. [31].

In addition, control experiments were carried out, in order to evaluate the ability of PMS to degrade IBU in the absence of a catalyst, and the adsorption capacity of both the support and the catalysts. The catalytic activity of Z support was also evaluated.

To determine the mineralization degree, total organic carbon (TOC)

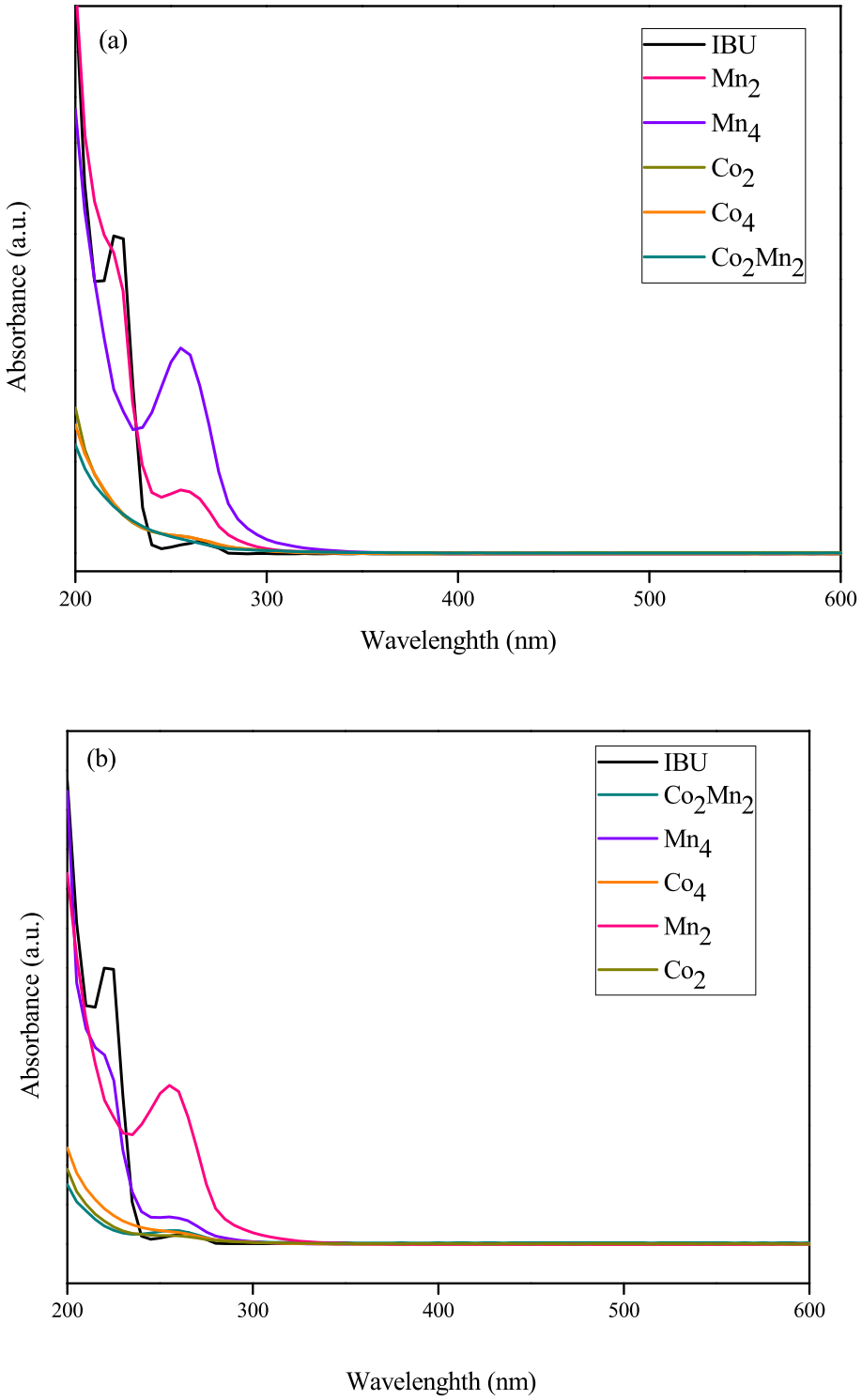


Fig. 3. UV–Vis profiles of IBU and degradation profiles for all catalysts. (a) Using 50 mg of catalyst mass and 49.4 mg PMS, (b) Using 100 mg of catalyst mass and 49.4 mg PMS (303 K, 4 h).

measurements were made with a TOC-LCPH/CPN analyzer (Shimadzu). The percentage of mineralization was calculated according to the following relationship:

$$\%\text{mineralization} = \frac{(TOC_0 - TOC_t)}{TOC_0} \times 100 \quad (1)$$

where TOC_0 (mg/ L) is the total organic carbon of the IBU initial solution and TOC_t (mg/ L) is the total organic carbon concentration at reaction time t.

The leaching of Co and Mn ions in the residual solutions was also determined using a GBC Avanta Model B-932 Atomic Absorption Spectrometer.

In order to assess the stability of the catalysts, the reusability of certain samples was investigated following the procedure outlined. After the initial run, the solid component was isolated from the reaction mixture through filtration, subjected to a distilled water rinse, and

Table 3
Percentage of mineralization and metal leaching in the reaction residual liquids after 4 h of reaction.

Catalysts	Catalyst mass (mg)	% Mineralization	Metal leaching (g%)	
			Co	Mn
Co_2	50	42.6	13.1	–
	100	50.4		
Mn_2	50	< 10	–	3.32
	100	< 10		
Co_2Mn_2	50	56.7	27.3	5.11
	100	37.9		
Co_4	50	50.4	5.77	–
	100	34.0		
Mn_4	50	< 10	–	n.d
	100	23.6		

n.d.: not determined.

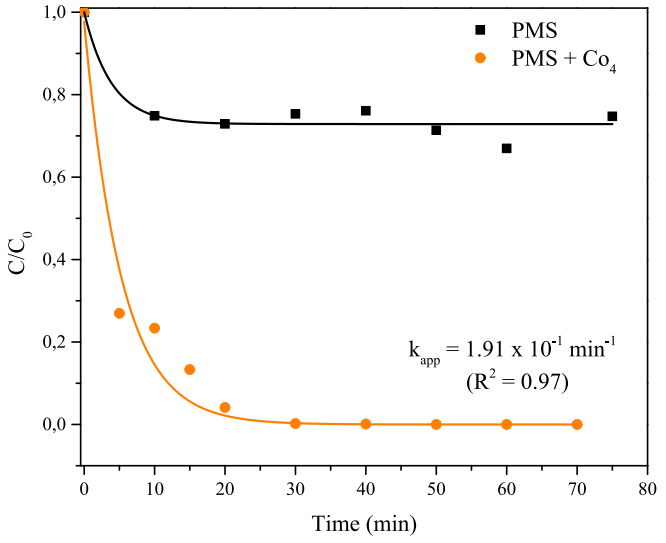


Fig. 4. Comparison of degradation kinetics of IBU with Co_4, and the control experiment with PMS alone (50 mg of catalyst, 74.3 mg PMS).

subsequently air-dried at ambient conditions. The catalyst was then used in a subsequent reaction cycle, maintaining a constant mass ratio catalyst:oxidant:IBU. This sequential process was repeated for a minimum of three iterations.

In order to determine the main radicals involved in the degradation of IBU, both experiments were conducted in the presence of tert-butanol (TbOH) and ethanol (EtOH), keeping constant the reaction proportions. The addition of alcohol followed a ratio of oxidant to alcohol of 1:150.

3. Results and discussion

3.1. Characterization of the catalysts

The metal content of the catalysts was determined by atomic absorption spectrometry and the results are shown in Table 2. The Co loading in the support using incipient wetness impregnation method was similar to the nominal content. In contrast, the Mn content was substantially lower than the nominal in both mono- and bimetallic catalysts.

The chemical analysis of the metal content is in agreement with the EDS results. In addition, it has been verified that not only is the content comparable, but the distribution of the metals on the support material is also uniform (Fig. S1, Suppl. Mater.).

Fig. 1 shows the XRD profiles of the prepared samples. The profiles show only the diffraction peaks of the zirconia crystal structure in the tetragonal phase (JCPDS 79–1769). In the case of the monometallic Co_2 and Co_4 catalysts and the Mn_2 sample, an additional peak appears at 28.2°, attributed to traces of the monoclinic phase of the support (JCPDS 37–1484), marked with (*) in the Figure. None of the diffractograms show peaks attributed to Mn or Co oxides, which could be due to a high degree of dispersion of the metal species on the support.

Scherrer's formula was applied to compute the crystallite size (eq. 2).

$$D = \frac{K\lambda}{\beta\cos\theta} \quad (2)$$

where, D is the size of the particle, λ the wavelength (0.1542 nm, Cu-Kα radiation), β the full width at half maximum, and θ the Bragg angle. The average crystallite sizes of all samples, determined from the diffraction peaks indexed to the (110), (112), (211) and (220) planes of the tetragonal phase, are reported in Table 2. These values are in agreement with those reported for Z-based materials prepared by coprecipitation method [32].

Fig. 2 illustrates the FTIR spectra of the Z support and the Co_2Mn_2, Mn_4, Co_4, Mn_2 and Co_2 catalysts. The IR spectra of all the materials are similar. The support shows bands at 420, 501, 573 and 730 cm^{-1}, characteristic of Zr–O–Zr vibrations. The spectrum of Co_2 exhibits a decrease in the intensity of the bands at 420 and 573 cm^{-1} and the disappearance of the signal at 730 cm^{-1}. This fact could be due to the formation of Zr-O-Co bonds in the cobalt anchoring process to the

Table 4
comparative analysis of the catalytic efficiency of Co4 with previously reported studies on the degradation of IBU.

Catalyst	IBU concentration	Experimental conditions	k (min^{-1})	IBU removal	TOC	Ref.
N-Co/D001CB	10 ppm	25 °C, pH 4.5, [PMS] = 0.7 mM, 0.3 g/L catalyst	0.048	~97% after 60 min	n.i.	[37]
Co/D001CB	10 ppm	25 °C, pH 7, [PMS] = 0.7 mM, 0.3 g/L catalyst	0.216	70% after 60 min	n.i.	[38]
$MnCo_2O_4$/FCNTs	10 ppm	25 °C, pH 4.7, [PMS] = 0.07 mM, 0.1 g/L catalyst	0.285	~100% after 15 min	90%	[39]
Co_3O_4-rGO	30 ppm	Temperature not informed, pH 7, [PMS] = 2 mM, 0.15 g/L catalyst	0.117	98.3% after 30 min	39.2	[40]
Co-doped carbon matrix derived from peat	10 ppm	25 °C, pH 7.5, [PMS] = 2 mM, 0.10 g/L catalyst	0.069	100% after 60 min	76.1% (5 h)	[4]
Co/ZrO_2	**40 ppm**	**30 °C, pH 3, [PMS] = 6.5 mM, 0.6 g/L catalyst**	**0.191**	**100% after 30 min**	**63.3% (4 h)**	**This work**
Fe/ZrO_2	10 ppm	70 °C, pH 3, [H_2O_2] = 30 mM, 0.4 g/L catalyst	n.i.	n.i.	80% (2.5 h)	[27]
Cu/ZrO_2	10 ppm	70 °C, pH 5, [H_2O_2] = 30 mM, 0.2 g/L catalyst	n.i.	n.i.	69% (2.5 h)	
$Cu\text{-}Fe/ZrO_2$	10 ppm	70 °C, pH 3–4, [H_2O_2] = 30 mM, 0.2 g/L catalyst	n.i.	n.i.	~70–80% (2.5 h)	[29]
Fe/ZrO_2	10 ppm	70 °C, pH 5, [H_2O_2] = 24.5 mM, 0.25 g/L catalyst	n.i.	97%	40% (2 h)	[28]
Cu/ZrO_2	10 ppm	70 °C, pH 5, [H_2O_2] = 24.5 mM, 0.25 g/L catalyst	n.i.	100%	53% (2 h)	

n.i.: not informed

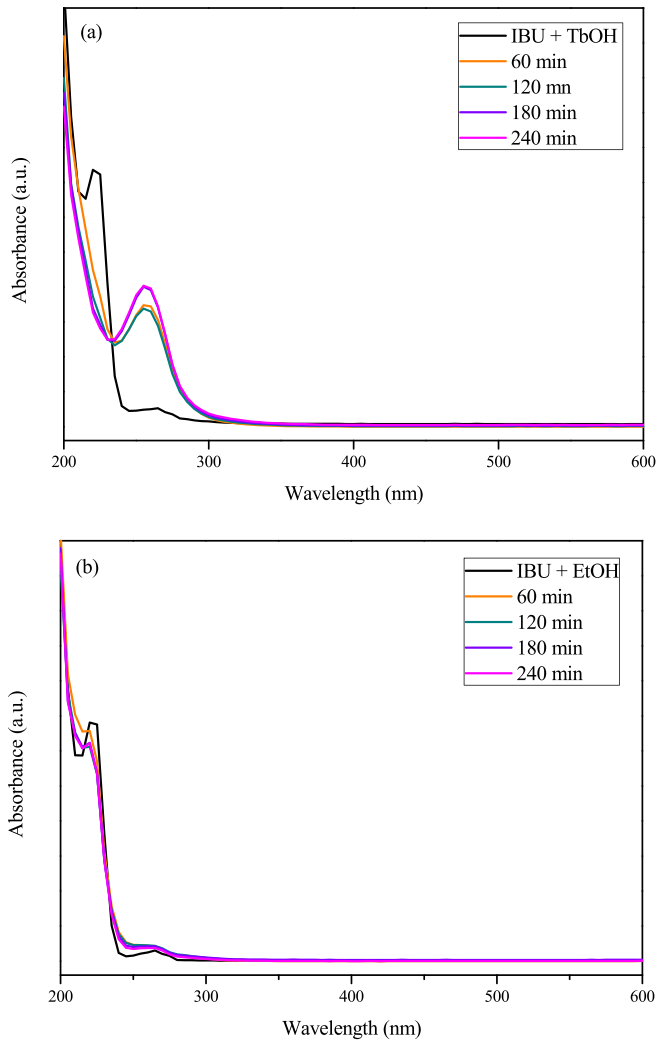


Fig. 5. UV–Vis profiles of IBU and experiences of identification of the radicals, using 50 mg of Co_4 and 49.4 mg PMS, at 303 K, for 240 min; (a) with TbOH (b) with EtOH.

surface of the support, which would generate some rigidity in the Zr—O bonds [33–35]. In the remaining IR spectra of the other catalysts, these bands are completely absent, confirming the effective anchoring of the metal species to the surface of the support material.

3.2. Catalytic activity

3.2.1. Control experiences

The control experiments employing only PMS, without the presence of any catalyst in the reaction media, showed no significant changes in the UV–Vis spectral profile of the original IBU solution and after 240 min of reaction. This result indicates that IBU cannot be efficiently degraded by PMS alone under the studied conditions (Fig. S2, Suppl. Material).

In order to evaluate the potential adsorption of IBU on both the support and the catalysts, experiments were carried out in which the solution of the pollutant was brought into contact with the mass of catalyst used in the catalytic reactions, in the absence of oxidant (Fig. S3 a and b, Suppl. Material). In both cases, the UV–Vis profile of the IBU did not undergo significant changes, which would be indicative of a low level of adsorption of the emerging pollutant on the solids. Moreover, in the evaluation of the catalytic activity of the Z support (without metal), only slight changes in the UV–Vis profile of IBU were observed after the same reaction time (Fig. S4, Suppl. Material).

In summary, the Z support exhibited minimal IBP conversion in the absence of PMS, indicating the absence of any significant oxidation activity of the material under these conditions. Additionally, it can be concluded that there were no significant adsorption effects of the pollutant on the catalyst surface.

3.2.2. Degradation experiences using PMS as an oxidizer

The simultaneous presence of catalysts and oxidant resulted in a significant improvement in the degradation rate of IBU. Fig. 3 shows the UV profiles of the initial IBU solution and the evolution of its oxidation with PMS with the mono- and bimetallic catalysts, with different masses of catalysts employed in this study, after 4 h of reaction. The UV–Vis spectrum of IBU exhibits distinctive bands at 221.5 nm and 265 nm, which can be attributed to $\pi \rightarrow \pi^*$ transitions derived from the aromatic ring within the IBU molecular structure. As the degradation reaction progresses, changes in the spectral features become apparent. Specifically, the band with higher intensity at 221.5 nm gradually reduces in intensity, while the band at 265 nm exhibits an increase in intensity. Moreover, the maximum absorption of the 265 nm band shifts towards shorter wavelengths as the reaction progresses. In particular, the monometallic Mn catalysts show the lowest activity under the experimental conditions studied. On the other hand, when reacting with Co-containing catalysts (namely Co_4, Co_2Mn_2, and Co_2), the intensity of the 265 nm band eventually decreases and finally disappears.

While it is observed that there is no significant change in the spectral profiles for the latter catalysts, regardless of the mass used, it is important to note that the primary difference in degradation efficiency becomes evident when examining the mineralization results, presented in Table 3.

When employing the Co_2 catalyst, mineralization values of up to 50% were achieved, indicating a relatively high level of degradation efficiency. Conversely, the Mn_2 catalyst yielded lower mineralization results. Interestingly, when both Co and Mn species were present in the Co_2Mn_2 sample, the level of mineralization decreased significantly, despite the observation of UV spectra free of bands attributable to aromatic fragments. In addition, the Mn_4 catalyst displayed inefficiency in mineralizing IBU under the studied conditions.

To investigate the potential leaching of metal cations, the residual liquids obtained from all the degradation experiments were analyzed by Atomic Absorption Spectroscopy (AAS), and the results are presented in Table 3. The data showed that the leachate from the waste liquids contained approximately 5% or even lower levels of Mn, depending on the material. In contrast, the Co catalysts exhibited higher leaching percentages, although the monometallic catalyst (Co_2) showed lower leaching compared to the bimetallic formulation (Co_2Mn_2) with a similar loading. This fact would suggest that the presence of Mn may weaken the Co species on the Z surface. It is noteworthy that among the catalysts tested, the monometallic Co_4 catalyst showed the highest stability in terms of leaching.

In view of the results presented in Table 3, which indicate that the use of less Co_4 catalyst resulted in mineralization of around 50%, a new experiment was carried out in which the amount of oxidant used was varied by increasing the dosage to 74.3 mg PMS (150 mg Oxone®). The results showed a significant improvement, with a mineralization value of 63.3% before complete consumption of the oxidant.

To evaluate the possibility of homogeneous catalysis due to the Co^{2+} ion leaching, an IBU degradation experiment was carried out with the addition of a certain volume of $Co(NO_3)_2$ (ac) in order to have the same metal content as the leachate for Co_4 (see Table 3). The degree of IBU mineralization achieved was ca. 34%, confirming the higher activity of the heterogeneous cobalt-based catalyst (UV–Vis spectra of the kinetic experience are shown in Fig. S5, Suppl. Material).

The latter IBU degradation was also evaluated through fluorescence spectroscopy. These results, together with the degradation of IBU with PMS alone, are shown in Fig. 4 (Fluorescence spectra of IBU degradation are shown in Fig. S6, Suppl. Material).

The control test (without catalyst addition) showed that PMS alone

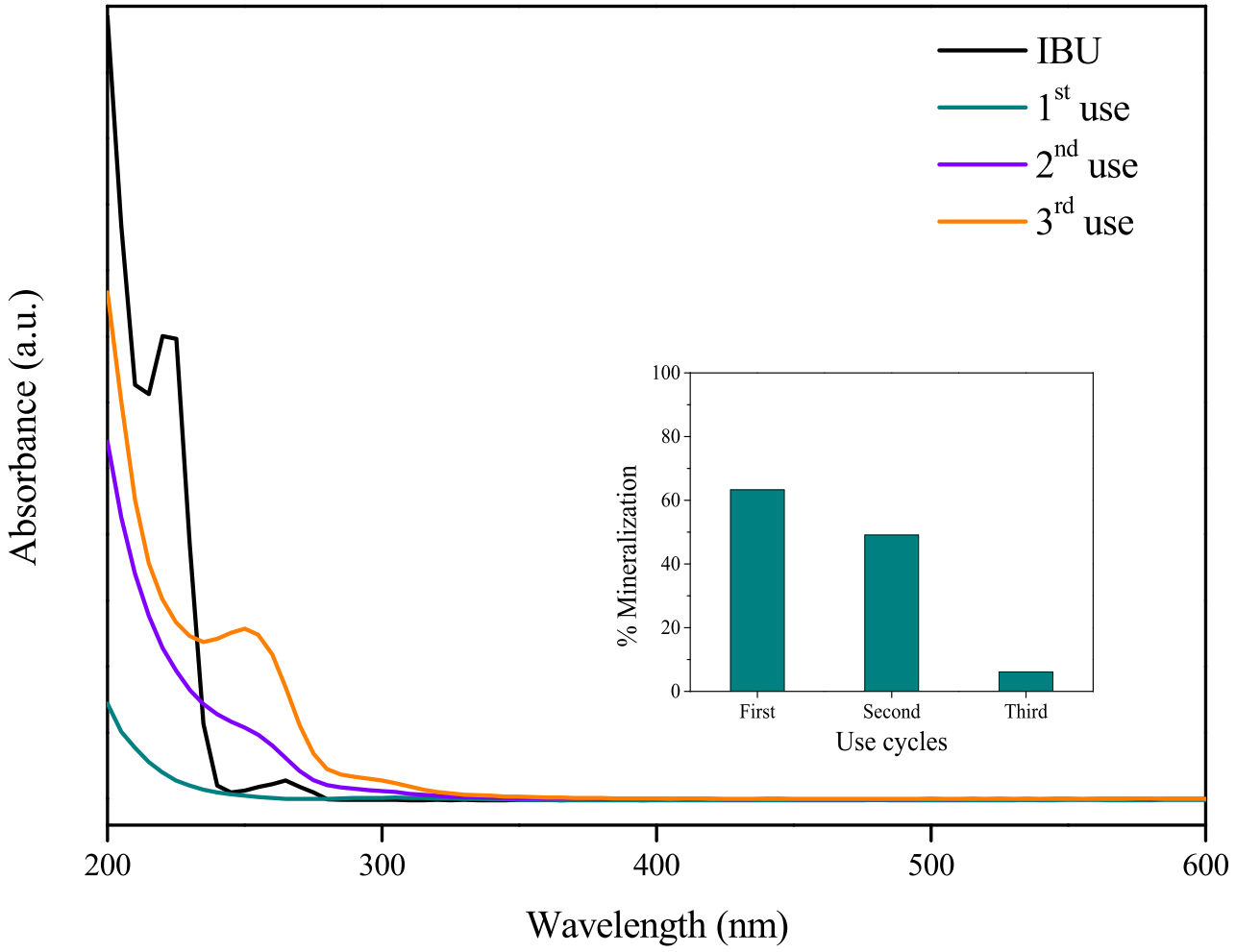


Fig. 6. UV–Vis profiles of IBU and three use cycles for Co_4. Inset: degree of mineralization of each cycle. (50 mg of catalyst, 74.3 mg PMS, 303 K, 4 h of reaction).

cannot completely decompose IBU under the studied conditions. This fact is consistent with the results obtained by Liu et al. (2020) [36]. Conversely, the Co_4 exhibited a complete IBU degradation in 30 min. The catalytic degradation follows a pseudo-first order kinetic reaction; its kinetics can be expressed as follows:

$$ln\left(\frac{C}{C_0}\right) = -kt \quad (3)$$

where C_0 and C represent the initial IBU concentration and the concentration (mg/L) at time t (min), respectively, and k is the reaction rate constant. The aforementioned results demonstrate the proficient degradation of IBU by Co_4, as evidenced by a rate constant of 1.91×10^{-1} min^{-1}.

Table 4 presents a comparative analysis of the catalytic efficiency of Co_4 with previously reported studies on the degradation of IBU. The comparison includes Co catalysts supported on different materials, as well as other metal catalysts supported on Z. The results indicate that our Co catalyst demonstrates exhibits really good performance, especially considering the lack of any pH control other than the final pH achieved by the addition of PMS, the near ambient temperature, and the simple method of catalyst preparation.

3.2.3. Radical scavengers and possible activation mechanism

Classical scavenger quenching tests were performed to determine the contributions of the major radicals involved in the degradation of IBU. TbOH and EtOH and were used as scavengers for only $^{\bullet}OH$ and all radicals ($^{\bullet}OH$ and $SO_4^{\bullet-}$), respectively (Fig. 5).

In the case of the reaction conducted in the presence of EtOH, the degradation profile of IBU exhibits negligible changes after a reaction time of 4 h. Conversely, when TbOH, a selective scavenger of $^{\bullet}OH$ radicals, was used, a spectral profile with more pronounced degradation was observed compared to the EtOH experiment. This observation not only indicates the occurrence of the reaction via the radical pathway but also suggests that the $SO_4^{\bullet-}$ radical dominates the transformation of IBU.

Thus, the mechanism of activation of PMS by Co_4 for radical production and organic degradation can be summarized as follows:

$$Z \equiv Co^{II} + HSO_5^- \rightarrow Z \equiv Co^{III} + SO_4^{\bullet-} + OH^- \quad (4)$$

$$Z \equiv Co^{III} + HSO_5^- \rightarrow Z \equiv Co^{II} + SO_5^{\bullet-} + H^+ \quad (5)$$

$$SO4^{\bullet-} + H_2O \rightarrow SO_4^{2-} + {}^{\bullet}OH + H^+ \quad (6)$$

$$SO_4^{\bullet-}\ (\text{and/or}\ {}^{\bullet}OH) + \text{IBU} \rightarrow \text{degradation intermediates} \rightarrow CO_2 + H_2O \quad (7)$$

The generation of $SO_4^{\bullet-}$ occurs through homolytic cleavage of the PMS peroxide group (O—O) by accepting an electron from the cobalt of the catalyst surface (Eq. 4). The resulting $SO_4^{\bullet-}$ species have an E^0 value of 2.60 V, which is higher than that of HSO_5^- ($E^0 = 1.75$ V), making it a more effective oxidant for the degradation of organic pollutants. At the same time, the oxidized cobalt on the catalyst surface can be reduced back to its original oxidation state via a one-electron reduction process by PMS, producing a $SO_5^{\bullet-}$ radical, a weaker oxidant agent with an E_0 value of 1.10 V [41]. The net reaction can be expressed by combining Eqs. 4 and 5 as follows:

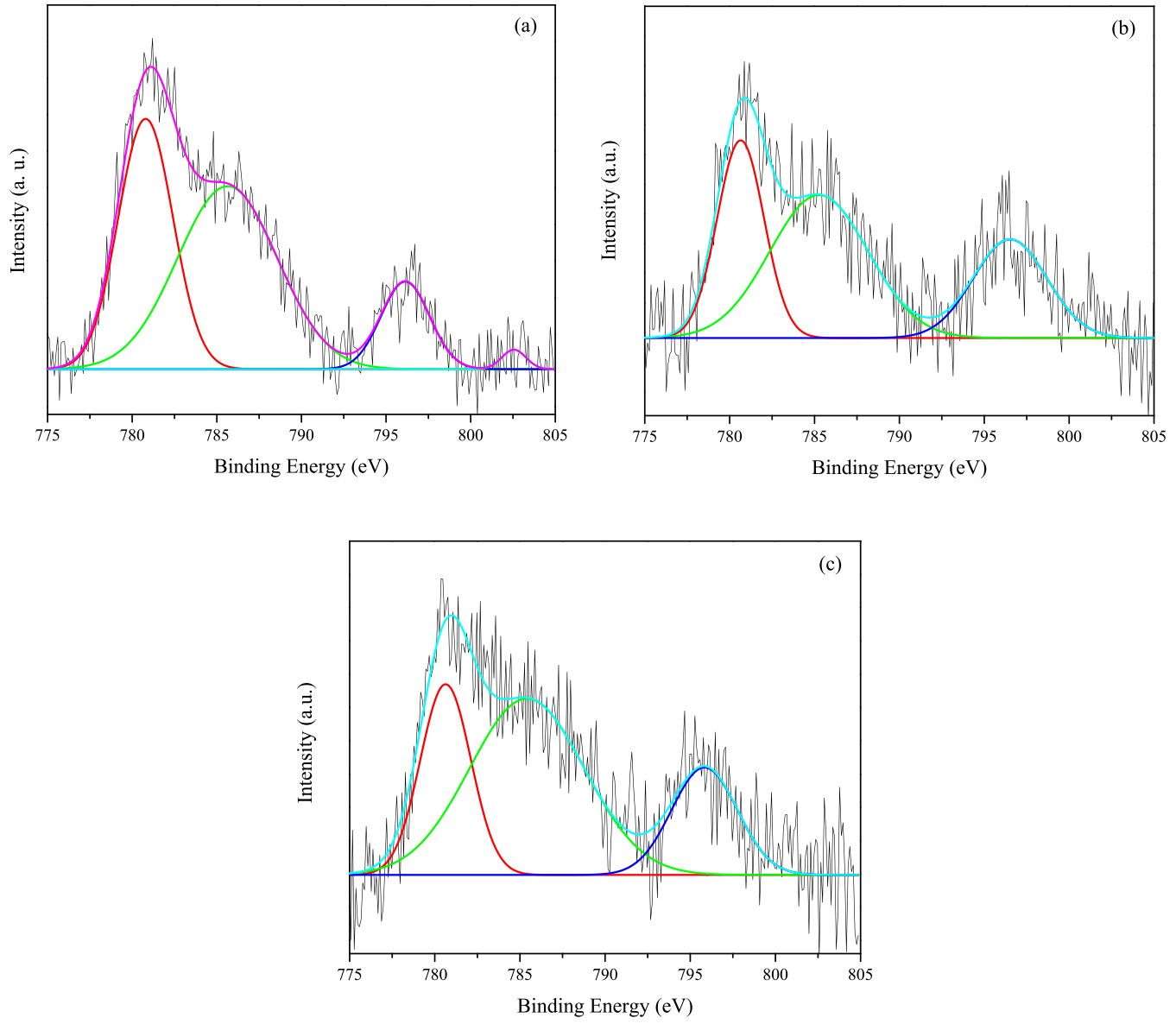


Fig. 7. XPS Co2p spectra of the Co_4 catalyst. a) As prepared, b) after the first use in reaction, and c) after the second use in reaction (50 mg of catalyst, 74.3 mg PMS, 303 K, 4 h of reaction).

$$2\,HSO_5^- \rightarrow SO_5^{\bullet -} + SO_4^{\bullet -} + H_2O \quad (8)$$

3.2.4. *Reusability tests*

The reusability of the Co_4 catalyst was also investigated in successive cycles with a catalyst to PMS ratio of 50 mg and 74.3 mg, respectively (Fig. 6). The results showed that this particular catalyst performed satisfactorily for up to two consecutive cycles with acceptable levels of mineralization.

Fig. 7a shows the high resolution XPS spectra of 2p Co for Co_4 fresh sample. Two peaks situated at binding energies of 780.8 eV (FWHM = 3.5) and 785.6 eV (FWHM = 5.6) corresponding to Co 2p3/2, and other two signals at 796.1 eV (FWHM = 3.4) and 802.6 eV (FWHM = 6.6) attributed to Co 2p1/2, are displayed. The presence of the satellite peaks indicates the existence of Co^{2+} species [42–44]. To estimate the relative proportion of Co^{2+} to Co, the ratios between the areas of the Co 2p3/2 satellite peak (I_{sat}) and the total area of the Co 2p3/2 signal ($I_{Co2p3/2}$) were calculated ($I_{sat}/I_{Co2p3/2} = 0.57$), according to Leonardi et al. [45]. The Co 2p spectra of the reused catalyst show a significant increase of satellite peaks, with ratios $I_{sat}/I_{Co2p3/2} = 0.63$ and 0.68 for the second and third cycle of use, respectively (Figs. 7b and c). These results indicate that Co^{2+} would still be the predominant surface species after IBU degradation reaction. Therefore, it is likely that the main reason for the decrease in catalytic activity observed after successive cycles of Co_4 use is the lower metal loading in the solid caused by the slight metal leaching after the reaction, instead of the oxidation of cobalt species on the surface of the catalyst.

4. Conclusion

Mono- and bimetallic Co—Mn catalysts supported on Z were synthesized, characterized and tested for the catalytic degradation of IBU, which was taken as a model of emerging pollutant. The Co_4 catalyst showed the highest performance, achieving a total IBU degradation after 30 min together with 63% mineralization levels after 4 h, and it could also be reused. This efficiency may be attributed to the cobalt content, rather than to the synergistic effect that may be present in the bimetallic catalyst. The degradation of the pollutant occurs by a radical mechanism, mainly governed by $SO_4^{\bullet -}$ radicals, and $^{\bullet}OH$ in a lesser extent.

Declaration of generative AI and AI-assisted technologies in the writing process

During the preparation of this work the author(s) used DeepL Write in order to improve language and English grammar. After using this tool/service, the author(s) reviewed and edited the content as needed and take(s) full responsibility for the content of the publication.

CRediT authorship contribution statement

Romina D. Goenaga: Data curation, Methodology, Writing – original draft. **Alejandra S. Diez:** Conceptualization, Investigation, Supervision. **Mariana Alvarez:** Conceptualization, Formal analysis, Funding acquisition, Investigation, Methodology, Project administration, Supervision, Writing – review & editing.

Declaration of competing interest

The authors declare the following financial interests/personal relationships which may be considered as potential competing interests:

Mariana Alvarez reports financial support was provided by National University of the South. Mariana Alvarez reports financial support was provided by Agencia Nacional de Promoción Científica y Tecnológica.

Data availability

Data will be made available on request.

Acknowledgments

The authors gratefully acknowledge Dr. German Prieto for his generous cooperation in the SEM-EDS measurements. R.D.G. has a fellowship of Universidad Nacional del Sur (UNS). A.S.D. is a UNS researcher. M.A. is a CONICET and UNS researcher. This work was funded by SGCyT-UNS 24/Q096 and PICT 2020–2308 research grants.

Appendix A. Supplementary data

Supplementary data to this article can be found online at https://doi.org/10.1016/j.catcom.2024.106844.

References

[1] S. Khalaf, J.H. Shoqeir, F. Lelario, L. Scrano, S.A. Bufo, R. Karaman, TiO_2 and active coated glass photodegradation of ibuprofen, Catalysts 10 (5) (2020) 560, https://doi.org/10.3390/catal10050560.
[2] J. Jan-Roblero, J.A. Cruz-Maya, Ibuprofen: toxicology and biodegradation of an emerging contaminant, Molecules 28 (5) (2023) 2097, https://doi.org/10.3390/molecules28052097.
[3] P. Izadi, et al., Non-steroidal anti-inflammatory drugs in the environment: where were we and how far we have come? Environ. Pollut. 267 (2020) 115370 https://doi.org/10.1016/j.envpol.2020.115370.
[4] Z. Ren, et al., Ibuprofen degradation using a Co-doped carbon matrix derived from peat as a peroxymonosulphate activator, Environ. Res. 193 (2021) 110564, https://doi.org/10.1016/j.envres.2020.110564.
[5] E.A. Tyumina, G.A. Bazhutin, A.D.P. Cartagena Gómez, I.B. Ivshina, Nonsteroidal anti-inflammatory drugs as emerging contaminants, Microbiology (Russian Federation) 89 (2) (2020) 148–163, https://doi.org/10.1134/S0026261720020125.
[6] A. Sandoval-González, I. Robles, C.A. Pineda-Arellano, C. Martínez-Sánchez, Removal of anti-inflammatory drugs using activated carbon from agro-industrial origin: current advances in kinetics, isotherms, and thermodynamic studies, J. Iran. Chem. Soc. 19 (10) (2022) 4017–4033, https://doi.org/10.1007/s13738-022-02588-7.
[7] E. Brillas, A critical review on ibuprofen removal from synthetic waters, natural waters, and real wastewaters by advanced oxidation processes, Chemosphere 286 (2022) 131849, https://doi.org/10.1016/j.chemosphere.2021.131849.
[8] V. Priyan, S. Narayanasamy, Effective removal of pharmaceutical contaminants ibuprofen and sulfamethoxazole from water by corn starch nanoparticles: an ecotoxicological assessment, Environ. Toxicol. Pharmacol. 94 (2022) 103930, https://doi.org/10.1016/j.etap.2022.103930.
[9] M. Ma, L. Chen, J. Zhao, W. Liu, H. Ji, Efficient activation of peroxymonosulfate by hollow cobalt hydroxide for degradation of ibuprofen and theoretical study, Chin. Chem. Lett. 30 (12) (2019) 2191–2195, https://doi.org/10.1016/j.cclet.2019.09.031.
[10] S. Sigonya, T.H. Mokhothu, T.C. Mokhena, T.R. Makhanya, Mitigation of non-steroidal anti-inflammatory and antiretroviral drugs as environmental pollutants by adsorption using nanomaterials as viable solution—a critical review, Appl. Sci. 13 (2) (2023) 772, https://doi.org/10.3390/app13020772.
[11] I. Ambriz-Mexicano, et al., Integrated adsorption and biological removal of the emerging contaminants ibuprofen, naproxen, atrazine, diazinon, and carbaryl in a horizontal tubular bioreactor, Bioprocess Biosyst. Eng. 45 (9) (2022) 1547–1557, https://doi.org/10.1007/s00449-022-02764-2.
[12] M. Olak-Kucharczyk, M. Foszpańczyk, R. Żyłła, S. Ledakowicz, Photodegradation and ozonation of ibuprofen derivatives in the water environment: kinetics approach and assessment of mineralization and biodegradability, Chemosphere 291 (2022) 132742, https://doi.org/10.1016/j.chemosphere.2021.132742.
[13] A. Marchlewicz, U. Guzik, K. Hupert-Kocurek, A. Nowak, S. Wilczyńska, D. Wojcieszyńska, Toxicity and biodegradation of ibuprofen by bacillus thuringiensis B1(2015b), Environ. Sci. Pollut. Res. 24 (8) (2017) 7572–7584, https://doi.org/10.1007/s11356-017-8372-3.
[14] S. Giannakis, K.Y.A. Lin, F. Ghanbari, A review of the recent advances on the treatment of industrial wastewaters by sulfate radical-based advanced oxidation processes (SR-AOPs), Chem. Eng. J. 406 (2021) 127083, https://doi.org/10.1016/j.cej.2020.127083.
[15] L. Martone, M. Minella, C. Minero, F. Sordello, D. Vione, Effective degradation of ibuprofen through an electro-Fenton process, in the presence of zero-valent iron (ZVI-EF), J. Clean. Prod. 367 (2022) 132894, https://doi.org/10.1016/j.jclepro.2022.132894.
[16] Y. Li, C. Chao, D. Zhang, Q. Chen, J. Sun, Removal of refractory organic pollutants by cobalt-doped graphene aerogel activated peroxymonosulfate oxidation, Mater. Sci. Semicond. Process. 150 (2022) 106956, https://doi.org/10.1016/j.mssp.2022.106956.
[17] R.H. Waldemer, P.G. Tratnyek, R.L. Johnson, J.T. Nurmi, Oxidation of chlorinated ethenes by heat-activated persulfate: kinetics and products, Environ. Sci. Technol. 41 (3) (2007) 1010–1015, https://doi.org/10.1021/es062237m.
[18] R. Dewil, D. Mantzavinos, I. Poulios, M.A. Rodrigo, New perspectives for advanced oxidation processes, J. Environ. Manag. 195 (2017) 93–99, https://doi.org/10.1016/j.jenvman.2017.04.010.
[19] X. Li, M. Zhou, Y. Pan, L. Xu, Z. Tang, Highly efficient advanced oxidation processes (AOPs) based on pre-magnetization Fe^0 for wastewater treatment, Sep. Purif. Technol. 178 (2017) 49–55, https://doi.org/10.1016/j.seppur.2016.12.050.
[20] S. Rahim Pouran, A.A. Abdul Raman, W.M.A. Wan Daud, Review on the application of modified iron oxides as heterogeneous catalysts in Fenton reactions, J. Clean. Prod. 64 (2014) 24–35, https://doi.org/10.1016/j.jclepro.2013.09.013.
[21] J. Rodríguez-Chueca, et al., Solar-assisted bacterial disinfection and removal of contaminants of emerging concern by Fe^{2+}-activated HSO_5^- vs. $S_2O_8^{2-}$ in drinking water, Appl. Catal. B 248 (2019) 62–72, https://doi.org/10.1016/j.apcatb.2019.02.018.
[22] S. Atalay, G. Ersöz, Springer Briefs in Molecular Science Green Chemistry for Sustainability Novel Catalysts in Advanced Oxidation of Organic Pollutants, 1st edition, Springer Ed, 2016.
[23] R.C. Weast, M.J. Astle, W.H. Beyer, CRC Handbook of Chemistry and Physics, 68th ed., CRC Press, Boca Raton, FL, 1987.
[24] DuPont™ Oxone® Monopersulfate Compound. General Technical Attributes https://www.waterguardinc.com/files/90708730.pdf (accessed 28 November 2023).
[25] W. Da Oh, T.T. Lim, Design and application of heterogeneous catalysts as peroxydisulfate activator for organics removal: an overview, Chem. Eng. J. 358 (2019) 110–133, https://doi.org/10.1016/j.cej.2018.09.203.
[26] D. Ma, et al., Critical review of advanced oxidation processes in organic wastewater treatment, Chemosphere 275 (2021) 130104, https://doi.org/10.1016/j.chemosphere.2021.130104.
[27] S. Hussain, E. Aneggi, A. Trovarelli, D. Goi, Heterogeneous Fenton-like oxidation of ibuprofen over zirconia-supported iron and copper catalysts: effect of process variables, J. Water Proc. Eng. 44 (2021) 102343, https://doi.org/10.1016/j.jwpe.2021.102343.
[28] S. Hussain, E. Aneggi, D. Goi, Enhanced ibuprofen removal by heterogeneous-Fenton process over cu/ZrO_2 and Fe/ZrO_2 catalysts, J. Environ. Chem. Eng. 8 (1) (2020) 103586, https://doi.org/10.1016/j.jece.2019.103586.
[29] S. Hussain, E. Aneggi, D. Goi, A. Trovarelli, Bimetallic cu/Fe catalysts for ibuprofen mineralization, Catalysts 11 (11) (2021) 1383, https://doi.org/10.3390/catal11111383.
[30] E.A. García, E.H. Rueda, A.J. Rouco, Sulfated zirconia catalysts promoted with Fe and Mn: Mn effect in the Fe dispersion, Appl. Catal. A: Gen. 210 (1–2) (2001) 363–370.
[31] S. Wacławek, K. Grübel, M. Černík, Simple spectrophotometric determination of monopersulfate, Spectrochim. Acta A Mol. Biomol. Spectrosc. 149 (2015) 928–933, https://doi.org/10.1016/j.saa.2015.05.029.
[32] A.S. Basaleh, S.I. El-Hout, M.H.H. Mahmoud, Li_2MnO_3@ZrO_2 heterojunctions for highly efficient catalytic photodegradation of atrazine herbicide, Ceram. Int. 48 (20) (2022) 30978–30987, https://doi.org/10.1016/j.ceramint.2022.07.059.
[33] M.M. Alqahtani, et al., Highly sensitive ethanol chemical sensor based on novel Ag-doped mesoporous α–Fe_2O_3 prepared by modified sol-gel process, Nanoscale Res. Lett. 13 (1) (2018) 157, https://doi.org/10.1186/s11671-018-2572-8.
[34] D. Pietrogiacomi, S. Tuti, M.C. Campa, V. Indovina, Cobalt supported on ZrO_2: catalysts characterization and their activity for the reduction of NO with C_3H_6 in the presence of excess O_2, Appl. Catal. B 28 (1) (2000) 43–54, https://doi.org/10.1016/S0926-3373(00)00161-2.

[35] R. Munirathinam, D. Pham Minh, A. Nzihou, Effect of the support and its surface modifications in cobalt-Based Fischer–Tropsch synthesis, Ind. Eng. Chem. Res. 57 (48) (2018) 16137–16161, https://doi.org/10.1021/acs.iecr.8b03850.
[36] Y. Liu, et al., Degradation of ibuprofen in soil systems by persulfate activated with pyrophosphate chelated Fe(II), Chem. Eng. J. 379 (2020) 122145, https://doi.org/10.1016/j.cej.2019.122145.
[37] C. Wang, G. Zhou, Y. Xu, P. Yu, Y. Sun, Nitrogen doped cobalt anchored on the used resin-based catalyst to activate peroxymonosulfate for the removal of ibuprofen, Water 14 (22) (2022), https://doi.org/10.3390/w14223754.
[38] G. Zhou, Y. Xu, X. Zhang, Y. Sun, C. Wang, P. Yu, Efficient activation of peroxymonosulfate by cobalt supported used resin based carbon ball catalyst for the degradation of ibuprofen, Materials 15 (14) (2022) 5003, https://doi.org/10.3390/ma15145003.
[39] C. He, C. Tang, W. Da Oh, Reinforced degradation of ibuprofen with $MnCo_2O_4$/FCNTs nanocatalyst as peroxymonosulfate activator: performance and mechanism, J. Environ. Chem. Eng. 10 (3) (2022) 107874, https://doi.org/10.1016/j.jece.2022.107874.
[40] C. Shen, Y. Wang, J. Fu, Urchin-like Co_3O_4 anchored on reduced graphene oxide with enhanced performance for peroxymonosulfate activation in ibuprofen degradation, J. Environ. Manag. 307 (2022) 114572, https://doi.org/10.1016/j.jenvman.2022.114572.
[41] W. Da Oh, Z. Dong, T.T. Lim, Generation of sulfate radical through heterogeneous catalysis for organic contaminants removal: current development, challenges and prospects, Appl. Catal. B 194 (2016) 169–201, https://doi.org/10.1016/j.apcatb.2016.04.003.
[42] H.L. Yuan, et al., Low-temperature preparation of superparamagnetic $CoFe_2O_4$ microspheres with high saturation magnetization, Nanoscale Res. Lett. 5 (11) (2010) 1817–1821, https://doi.org/10.1007/s11671-010-9718-7.
[43] J. Huang, W. Qian, H. Ma, H. Zhang, W. Ying, Highly selective production of heavy hydrocarbons over cobalt-graphene-silica nanocomposite catalysts, RSC Adv. 7 (53) (2017) 33441–33449, https://doi.org/10.1039/c7ra05887j.
[44] L.E. Gómez, A.V. Boix, E.E. Miró, Co/ZrO_2, co/CeO_2 and MnCoCe structured catalysts for COPrOx, Catal. Today 216 (2013) 246–253, https://doi.org/10.1016/j.cattod.2013.05.010.
[45] S.A. Leonardi, V.G. Milt, M.M. Fontanini, E.E. Miró, J.P. Bortolozzi, Cobalt oxide-based catalysts supported on zirconia fibers synthesized by atomic layer deposition, Mater. Chem. Phys. 294 (2023) 127043, https://doi.org/10.1016/j.matchemphys.2022.127043.